Nanomaterials

Lecture 1: Film Depositon Methods

Department of Materials Science and Engineering, Northwestern University

Film Deposition Methods

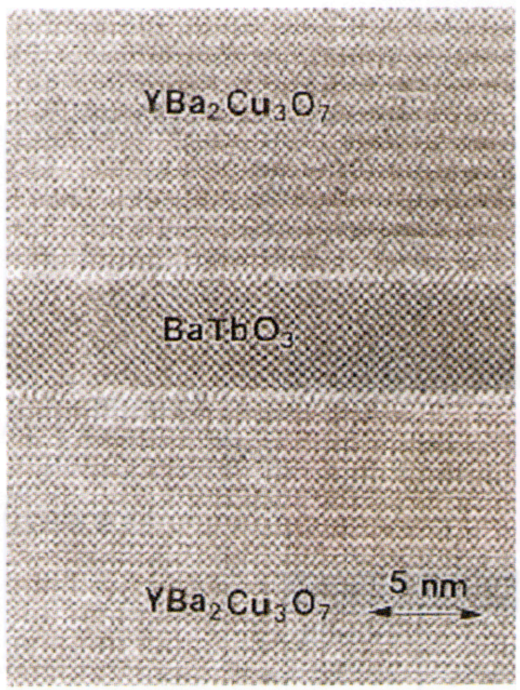

Figure 29: HRTEM micrograph of a sputter deposited trilayer system [19].

- Evaporation
- Molecular Beam Epitaxy
- Pulsed Laser Deposition
- Sputtering
- Chemical Vapor Deposition
- Atomic Layer Deposition

R. Waser (ed.), *Nanoelectronics and Information Technology*, Chapter 8

Influence of Background Vacuum Pressure

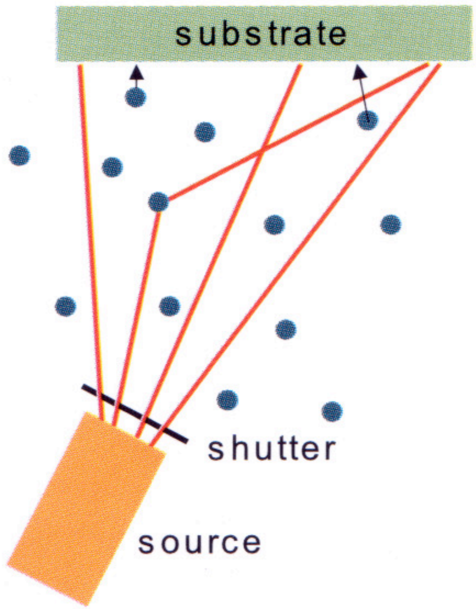

Figure 1: Schematics of a deposition system.

p (mbar)	Mean free path (cm)	Monolayers per sec
10^{0}	6.8×10^{-3}	3.3×10^{5}
10^{-3}	6.8×10^{0}	3.3×10^{2}
10^{-6}	6.8×10^{3}	3.3×10^{-1}
10^{-9}	6.8×10^{6}	3.3×10^{-4}

R. Waser (ed.), *Nanoelectronics and Information Technology*, Chapter 8

Deposition into Trenches

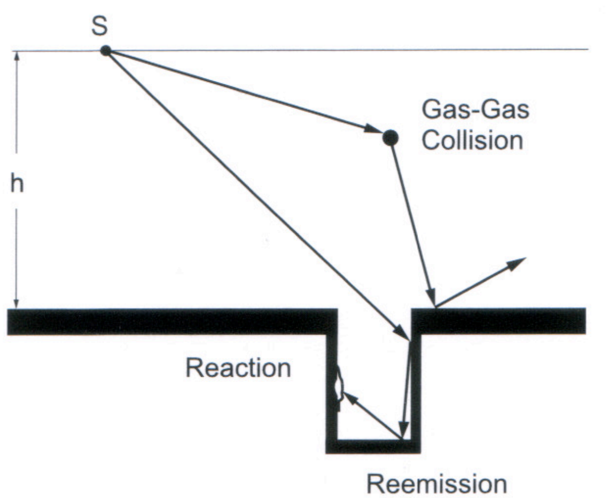

Figure 2: Deposition into a hole (after ref. 20). The example of an atom with starting position, S, with a height, h, above the substrate illustrates that either gas-gas collisions or reflection from the surface are necessary for a uniform deposition on bottom and sidewalls of a hole.

At low pressure, the mean free path can exceed the trench dimensions.

Consequently, surface reflections are necessary to achieve uniform deposition on the bottom and sidewalls of a trench.

R. Waser (ed.), *Nanoelectronics and Information Technology*, Chapter 8

Elements of Surface Morphology

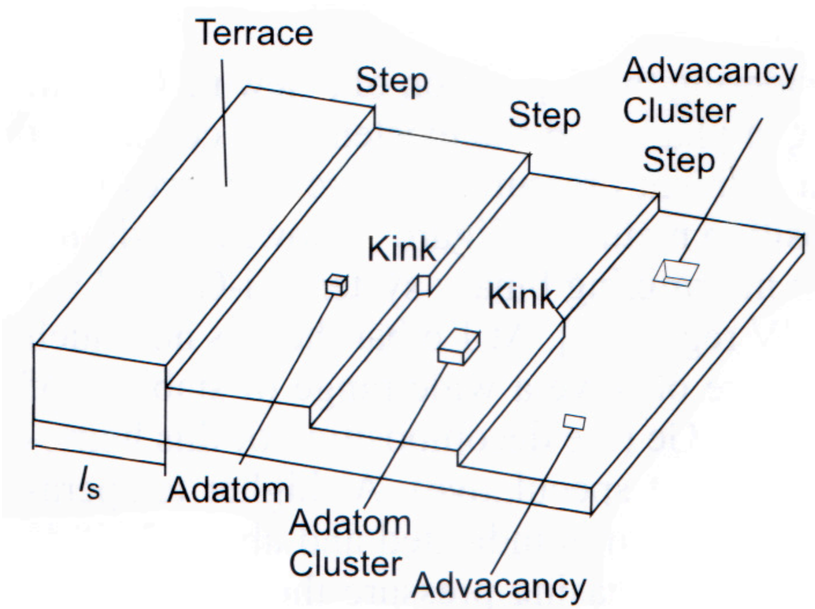

Figure 5: Schematic view of the elements of the surface morphology [3].

Nucleation and growth of a film proceeds from energetically favorable points on the substrate surface.

Even the cleanest polished surface shows some structure.

R. Waser (ed.), *Nanoelectronics and Information Technology*, Chapter 8

Homoepitaxy

Epitaxy: Growth of a film with the same crystal orientation as the substrate → "Single crystal on a single crystal"

Homoepitaxy: Film and substrate are the same material

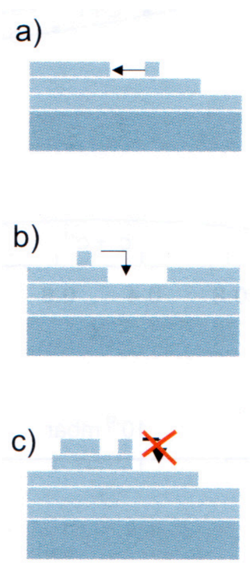

Growth modes of homoepitaxy:

(a) Step-propagation
(b) 2-D island growth
(c) Multi-layer growth

R. Waser (ed.), *Nanoelectronics and Information Technology*, Chapter 8

Heteroepitaxy

Heteroepitaxy: Film and substrate are different materials

Critical materials parameters that dictate growth mode:

(1) Surface energy, γ
(2) Lattice constants (lattice match)

If there is a lattice mismatch, there is a competition between strain energy ($\sim d^3$) and surface energy ($\sim d^2$):

$$\Delta W = W_{surf} + W_{relax} = C_1 \gamma d^2 - C_2 k \xi^2 d^3$$

where k = bulk modulus, ξ = strain

R. Waser (ed.), *Nanoelectronics and Information Technology*, Chapter 8

Lattice Mismatched Growth Mode

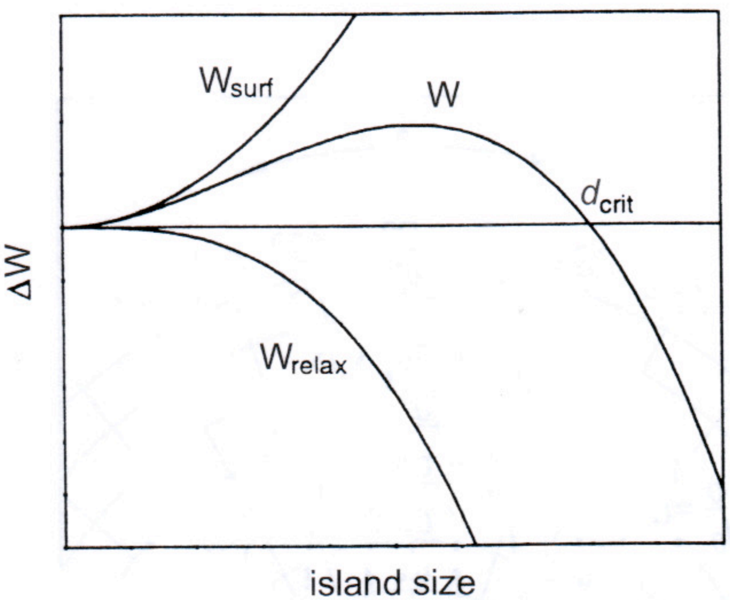

Figure 9: Energy contributions as a function of the island size [5].

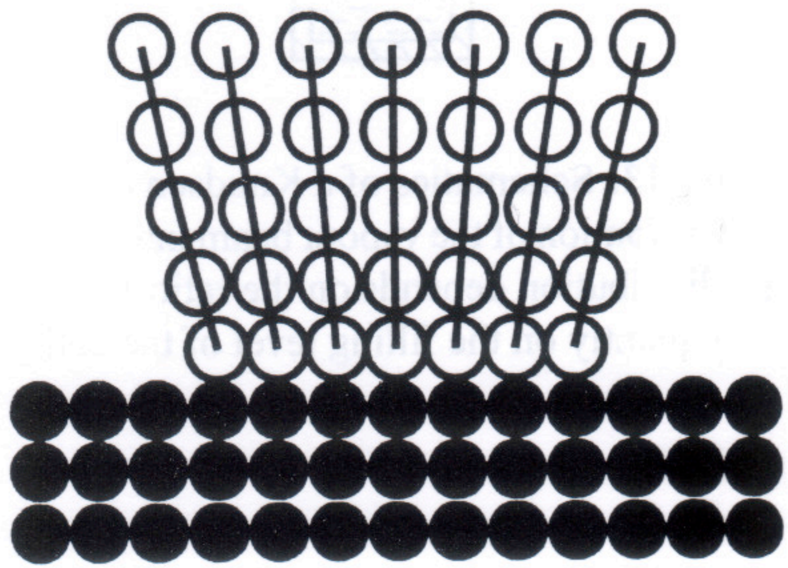

Figure 10: Strain relaxation in pseudo-morphic (dislocation - free) islands.

R. Waser (ed.), *Nanoelectronics and Information Technology*, Chapter 8

Classes of Heteroepitaxy Growth Modes

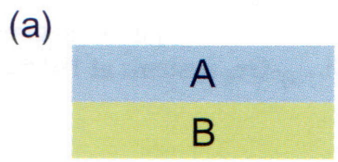

Frank-van der Merve

Lattice matched, $\gamma_{layer} + \gamma_{substrate/layer} < \gamma_{substrate}$

→ Perfect wetting and layer by layer growth

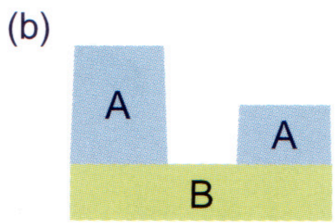

Volmer-Weber

Lattice matched, $\gamma_{layer} + \gamma_{substrate/layer} > \gamma_{substrate}$

→ Island growth

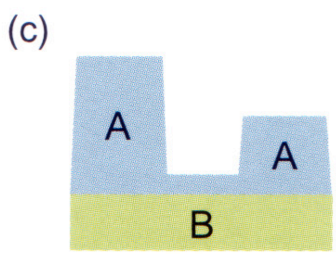

Stranski-Krastanov

Lattice mismatched

→ Layer by layer growth initially

→ When $d > d_{crit}$, island growth

R. Waser (ed.), *Nanoelectronics and Information Technology*, Chapter 8

Molecular Beam Epitaxy (MBE)

- Developed by A. Cho (UIUC alum) in 1971.
- Constituent elements in the form of molecular beams are deposited onto a heated substrate
- Molecular beams are formed from thermally evaporated sources
- Atomic level control is achieved via shuttering
- Resulting material has abrupt interfaces and exceptional control over thickness, doping, and composition

MBE Schematic

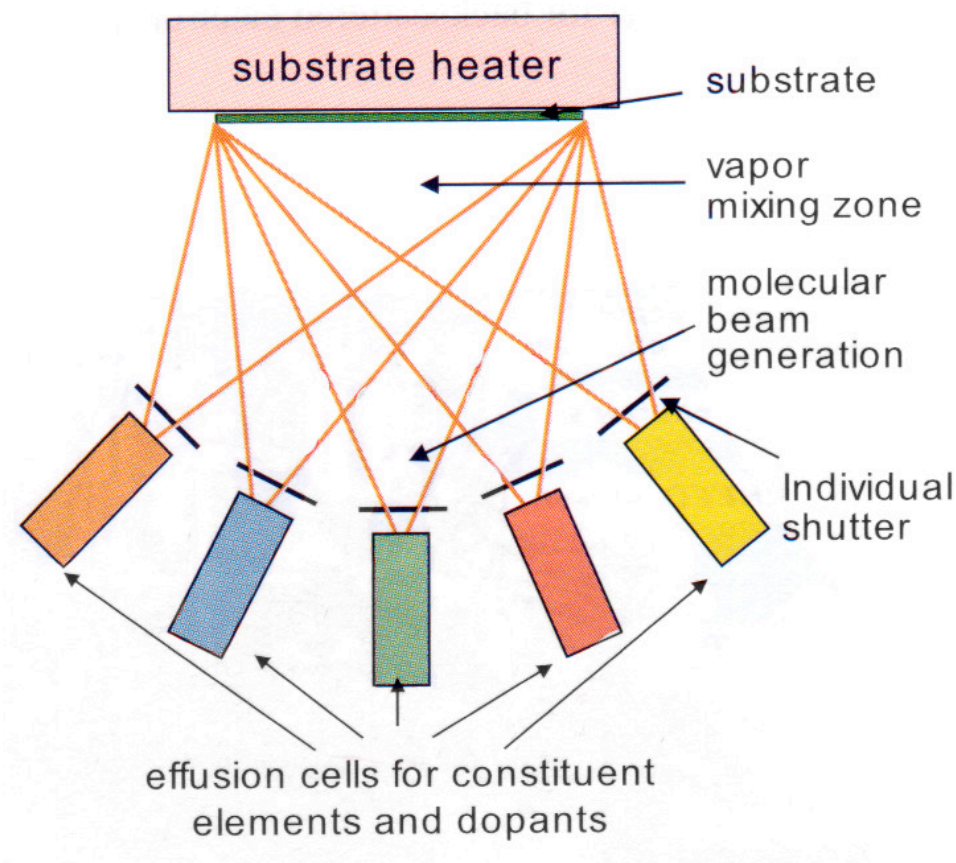

R. Waser (ed.), *Nanoelectronics and Information Technology*, Chapter 8

Characterization

(1) Electron diffraction → characterizes surface structure *in situ* during growth

(A) Low energy electron diffraction (LEED)

(B) Reflection high energy electron diffraction (RHEED)

(2) Cross-sectional microscopy → characterizes interfaces after growth

(A) Transmission electron microscopy (TEM) → structure and chemical composition

(B) Scanning tunneling microscopy (STM) → structure and electrical properties

Cross-sectional TEM image of GaAs/AlAs superlattice:

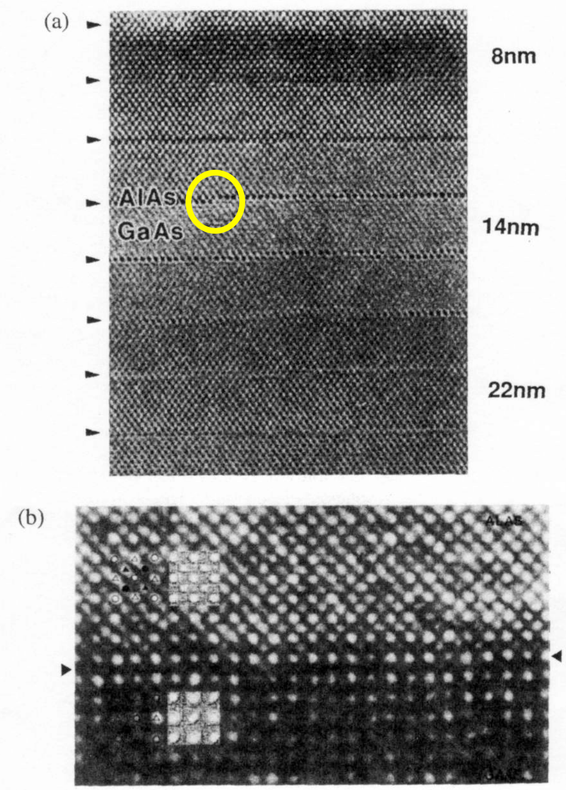

FIGURE 5. A cross-sectional TEM image of a *GaAs/AlAs* superlattice, in which one-monolayer thick *AlAs* and 10-monolayer thick *GaAs* were alternately deposited by MBE (after Ikarashi *et al.*[19]) (a). Another cross-sectional image of a *GaAs/AlGaAs* heterojunction (after Ichinose *et al.*[18]) (b). The image (a) was taken with the incident beam along the [100] direction, whereas the image (b) was made with the incident beam along the [110] direction.

G. Timp, *Nanotechnology*, Chapter 5

Cross-sectional STM images of GaSb/InAs superlattice:

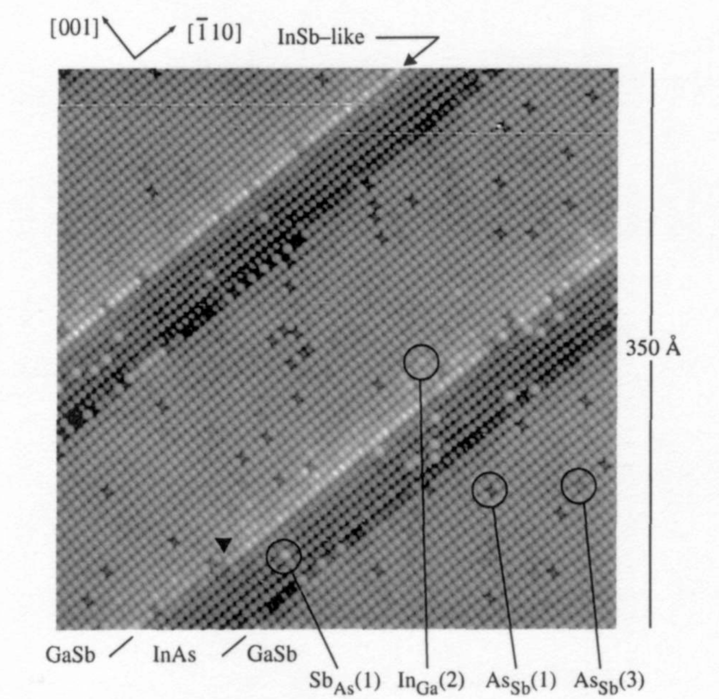

FIG. 1. Anion sublattice image of GaSb/InAs quantum wells in (110) cross section. InSb-like bonds account for the bright antimony layer along each GaSb-on-InAs interface. Growth direction is [001].

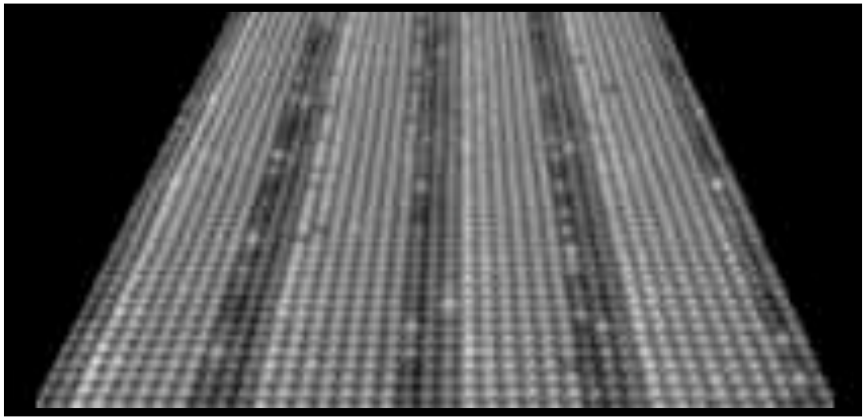

J. Steinshnider, *et al.*, *Phys. Rev. Lett.*, **85**, 2953 (2000).

Pulsed Laser Deposition (PLD)

Figure 20: Set-up of a pulsed laser deposition system for the deposition of oxide layers.

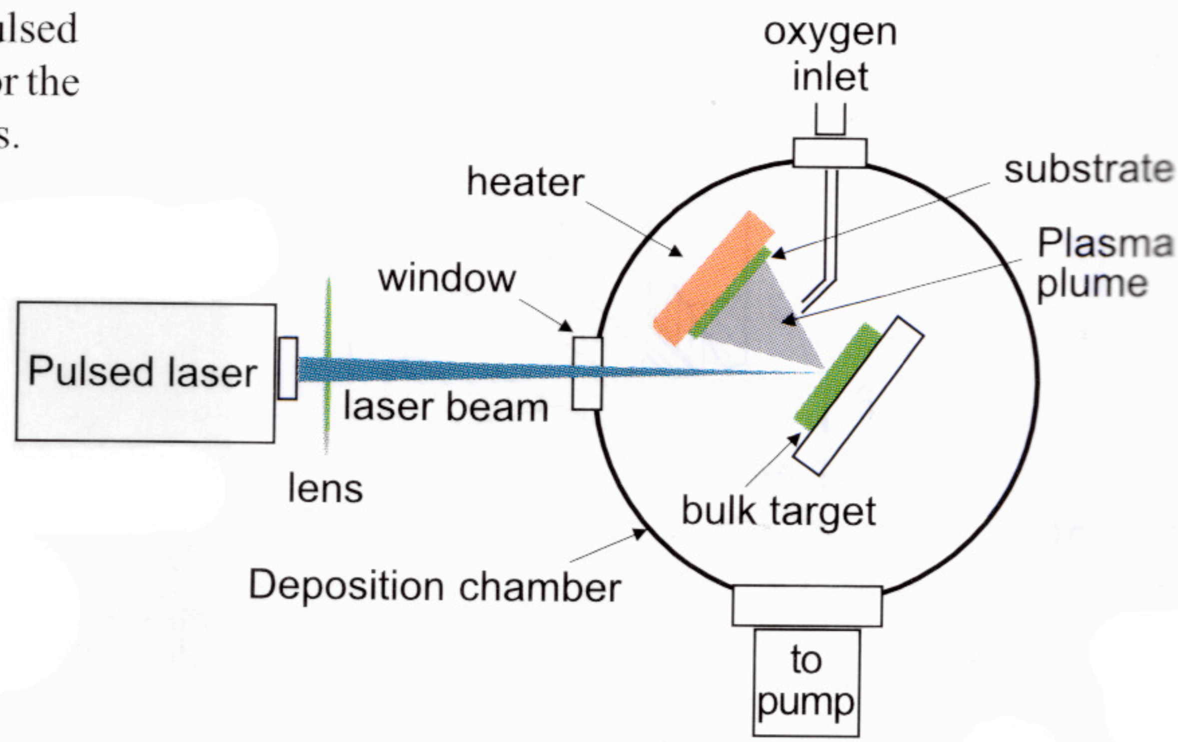

R. Waser (ed.), *Nanoelectronics and Information Technology*, Chapter 8

Time Evolution of the PLD Plasma Plume

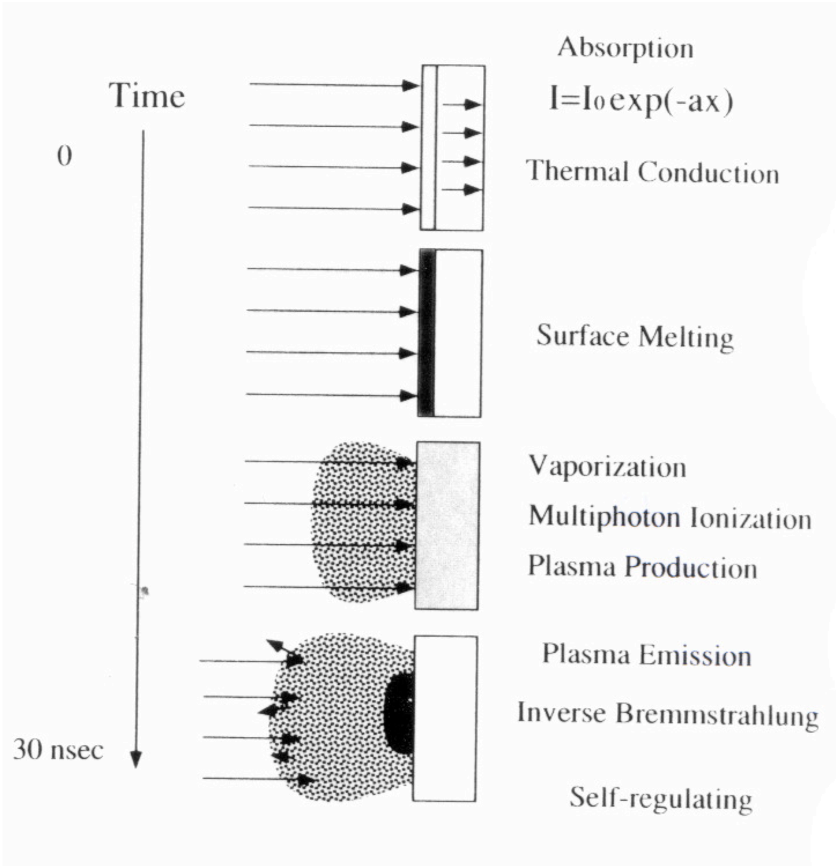

Figure 21: Time evolution of the plasma plume [10].

R. Waser (ed.), *Nanoelectronics and Information Technology*, Chapter 8

Sputter Deposition

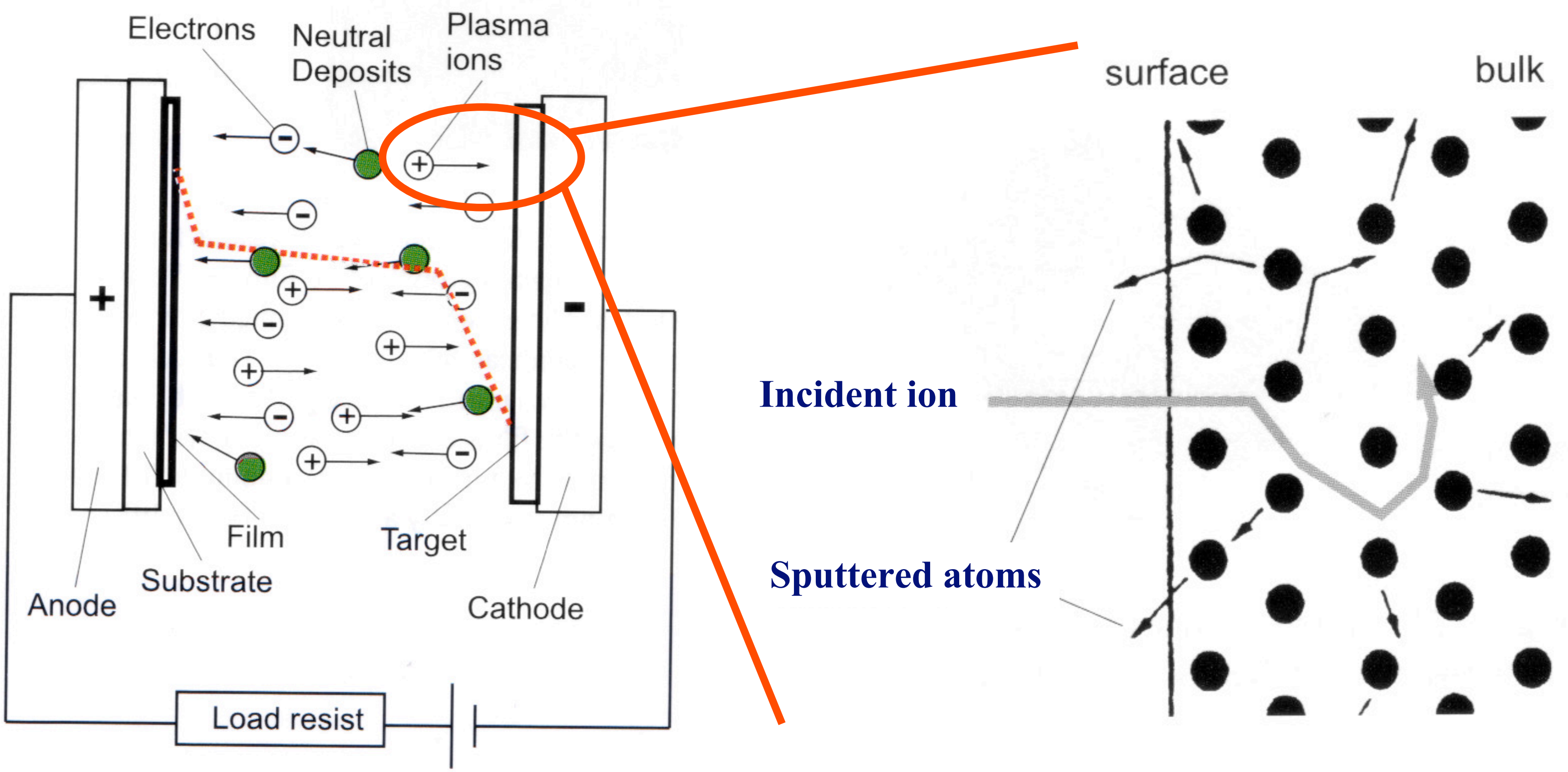

R. Waser (ed.), *Nanoelectronics and Information Technology*, Chapter 8

Pulsed Laser Deposition (PLD)

Figure 20: Set-up of a pulsed laser deposition system for the deposition of oxide layers.

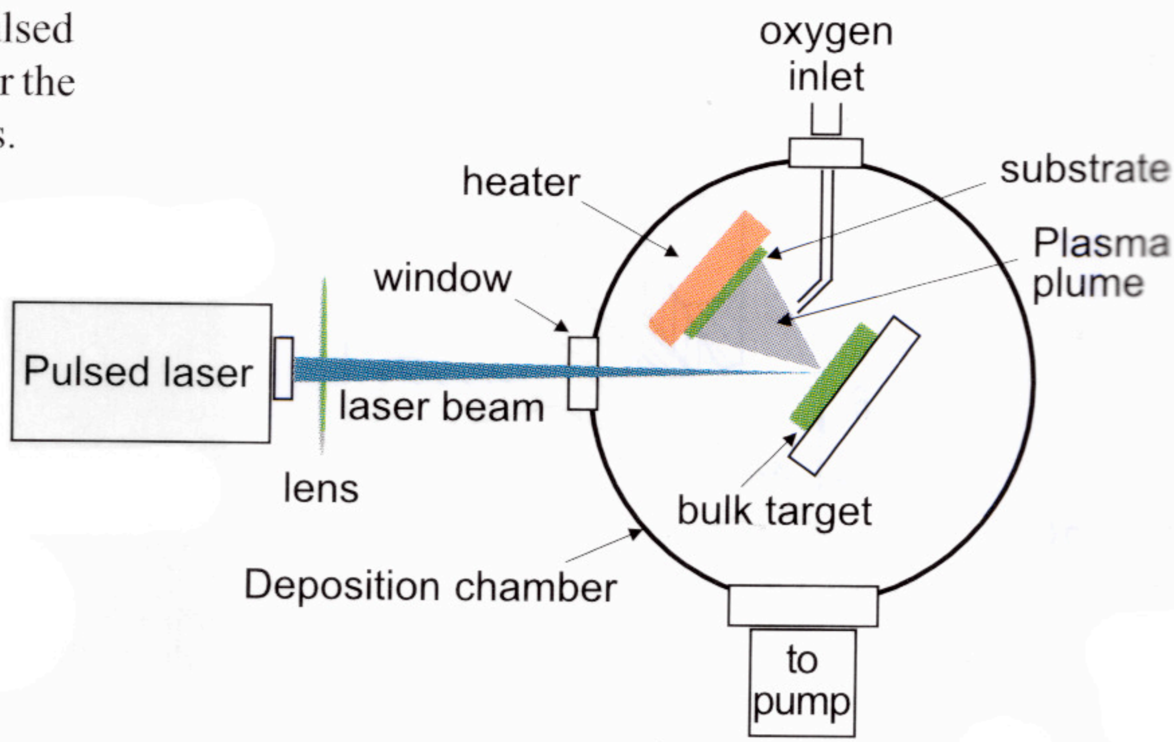

R. Waser (ed.), *Nanoelectronics and Information Technology*, Chapter 8

DC Sputter Deposition

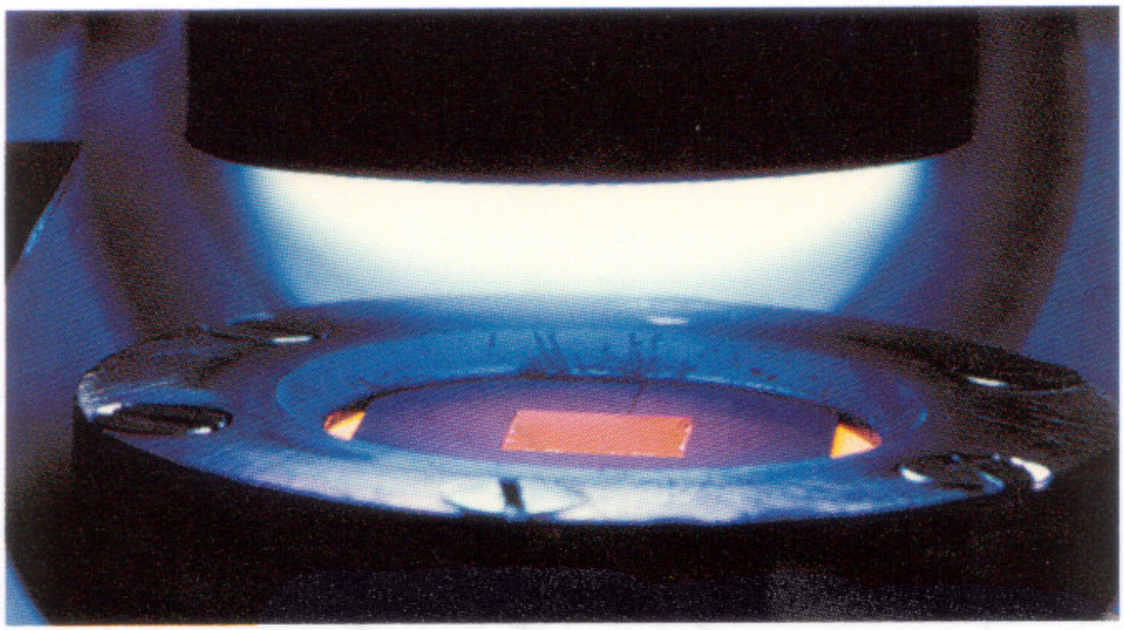

Figure 28: DC-sputter deposition in 'high pressure' oxygen.

R. Waser (ed.), *Nanoelectronics and Information Technology*, Chapter 8

Chemical Vapor Deposition (CVD)

- Source materials are delivered to the surface in the gas phase
- Energy is applied (heat, plasma, electromagnetic radiation)

→ Chemical bonds break → Free radicals react with substrate

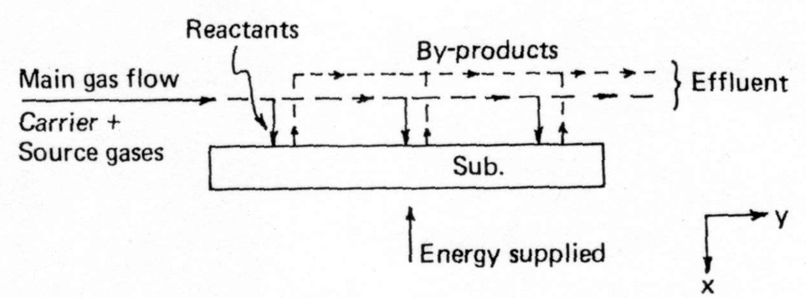

Figure 9–1. The basic mechanisms of a CVD system.

G. E. Anner, *Planar Processing Primer*, Chapter 9

Table 9–1. Typical CVD Processes and Reactions

Pyrolysis:

$$SiH_4\uparrow \rightarrow Si\downarrow + 2\,H_2\uparrow \quad \text{(a)}$$

$$SiH_2Cl_2\uparrow \rightarrow Si\downarrow + 2\,HCl\uparrow \quad \text{(a')}$$

Photolysis:

$$SiH_4\uparrow + 2\,N_2O \rightarrow SiO_2\downarrow + 2\,H_2\uparrow + 2\,N_2\uparrow \quad \text{(b)}$$

Reduction:

$$SiCl_4\uparrow + H_2\uparrow \rightarrow Si\downarrow + 4\,HCl\uparrow \quad \text{(c)}$$

$$SiHCl_3\uparrow + H_2\uparrow \rightarrow Si\downarrow + 3\,HCl\uparrow \quad \text{(c')}$$

Oxidation:

$$SiH_4\uparrow + O_2\uparrow \rightarrow SiO_2\downarrow + 2\,H_2\uparrow \quad \text{(d)}$$

Reduction-Oxidation:

$$3\,SiH_4\uparrow + 4\,NH_3\uparrow \rightarrow Si_3N_4\downarrow + 12\,H_2\uparrow \quad \text{(e)}$$

Doping Reactions:

$$n\,SiH_4\uparrow + B_2H_6\uparrow \rightarrow n\,Si\downarrow + 2\,B_2\downarrow + (2n+3)H_2\uparrow \quad \text{(f)}$$

$$n\,SiH_4\uparrow + 2\,PH_3\uparrow + n\,O_2\uparrow \rightarrow n\,SiO_2 + 2\,P\downarrow + (2n+3)H_2\uparrow \quad \text{(g)}$$

G. E. Anner, *Planar Processing Primer*, Chapter 9

Metal-Organic CVD (MOCVD)

Relies on organometallic precursor compounds:

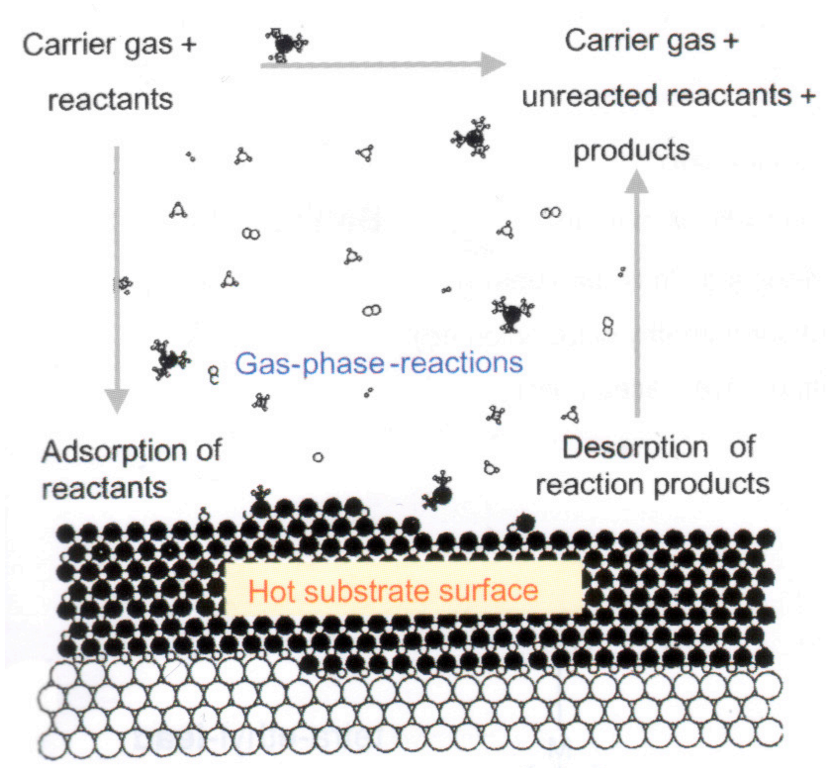

R. Waser (ed.), *Nanoelectronics and Information Technology*, Chapter 8

Atomic Layer Deposition

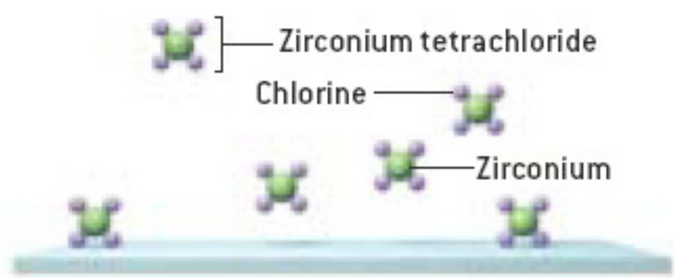

1 The surface is exposed to the first of two gases, here zirconium tetrachloride ($ZrCl_4$).

2 Molecules of $ZrCl_4$ adhere to the surface but not to one another.

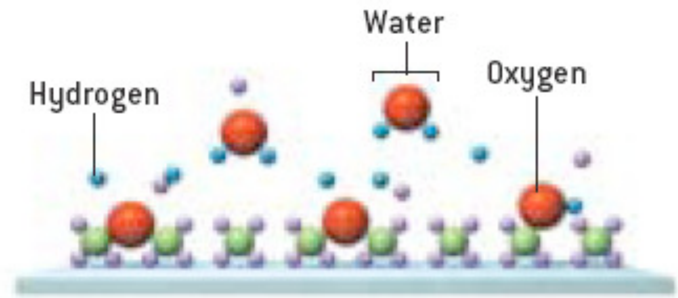

3 The coated surface is exposed to a second gas, in this case steam (H_2O).

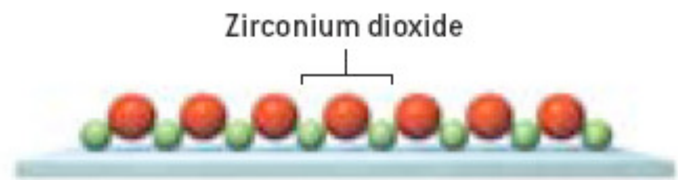

4 The $ZrCl_4$ on the surface reacts with the water (H_2O) to form a single-molecule-thick veneer of the desired material, zirconium dioxide (ZrO_2).

G. D. Hutcheson, *et al.*, *Scientific American*, **290**, 76 (2004).

Other Epitaxy Considerations

• In addition, defects in the underlying substrate will propagate into the growing film

(NOTE: Overgrowth can minimize defects – e.g., GaN on SiC)

• Periodic nanoscale defects will induce nanostructures in subsequent film growth. For example,

(1) Atomic steps
(2) Pre-patterned substrates

→ Although epitaxy always gives nanoscale control over 1-D, it can also provide 2-D and even 3-D control.

Epitaxial Lateral Overgrowth (ELOG)

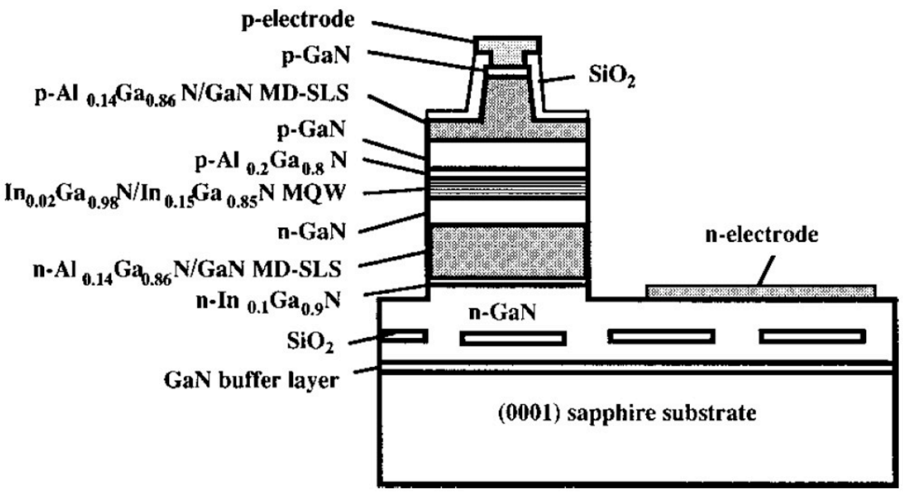

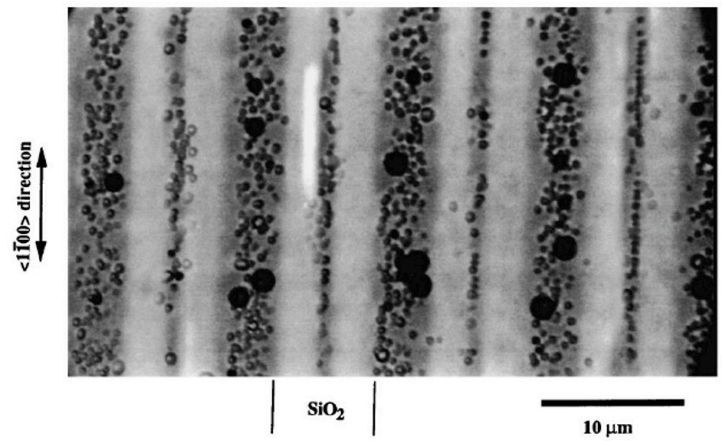

FIG. 1. Surface morphology after 4-μm etching of the ELOG substrate. The SiO_2 stripe width and window width were 7 μm and 4 μm, respectively. The etch pit density was about 2×10^8 cm^2 in the region of the 4-μm-wide stripe window.

Threading dislocations are dramatically reduced in the overgrowth region.

S. Nakamura, *et al.*, *Appl. Phys. Lett.*, **72**, 211 (1998).

2-D and 3-D Control by Epitaxy

Examples of structures grown by epitaxy:

(1) Ridge quantum wires → electrons confined to thicker regions (lower energy)

(2) Edge quantum wires → growth on cleaved heterostructure

(3) Self-assembled dots → form due to lattice mismatch in 2-D

(4) Self-assembled nanowires → form due to lattice mismatch in 1-D

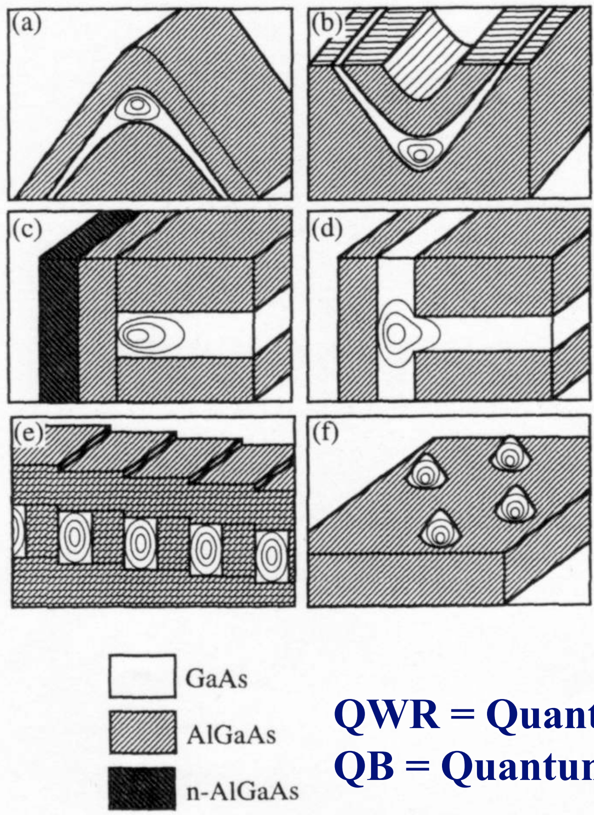

QWR = Quantum Wire
QB = Quantum Box

FIGURE 3. Examples of epitaxially grown QWRs and QBs. A ridge QWR (a), a groove QWR (b), a (field-induced) edge QWR (c), a (T-shaped) edge QWR (d), a tilted superlattice (TSL) (e), and a self-assembled QB structure (f). See section VI.B for their details and references.

G. Timp, *Nanotechnology*, Chapter 5

<u>NOTE</u>: Atomically controlled heterostructures have unique electronic and optical properties due to control of bandstructure:

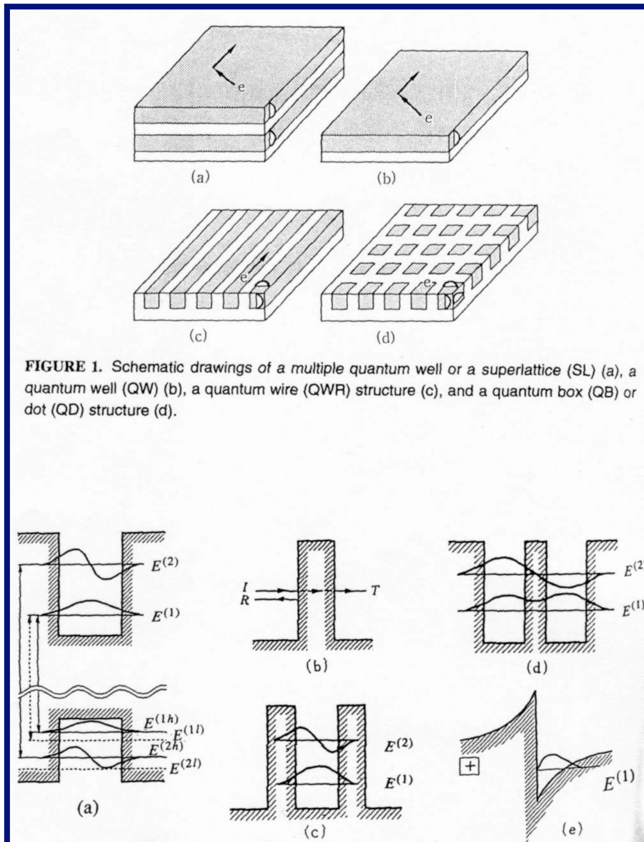

FIGURE 1. Schematic drawings of a multiple quantum well or a superlattice (SL) (a), a quantum well (QW) (b), a quantum wire (QWR) structure (c), and a quantum box (QB) or dot (QD) structure (d).

FIGURE 2. Potential profiles and eigenstates of electrons and holes in various quantum structures: (a) a quantum well (QW), (b) a single tunneling barrier, (c) a quantum well bound by double barriers, (d) a double (multiple) QW structure, (e) a heterojunction with an attractive field. Only in (a), the potential profile and eigenstates of heavy holes and light holes is shown.

G. Timp, *Nanotechnology*, Chapter 5

Quantum Mechanical Effects

1-D Time-independent Schrödinger Equation:

$$-\frac{\hbar^2}{2m}\frac{d^2\psi}{dz^2}+V\psi=E\psi$$

(1) Quantization of energy levels in wells

(2) Tunneling through barriers

→ When heterostructures are monolayers thick, atomic level defects have a serious impact

Quantum Mechanical Property Changes

Wells and tunnel barriers allow for quantum effects:

(1) Tailored optical properties

(2) Resonant tunneling diodes

(3) Single electron devices

(4) 2-dimensional electron gas

→ We will revisit these applications later in the course

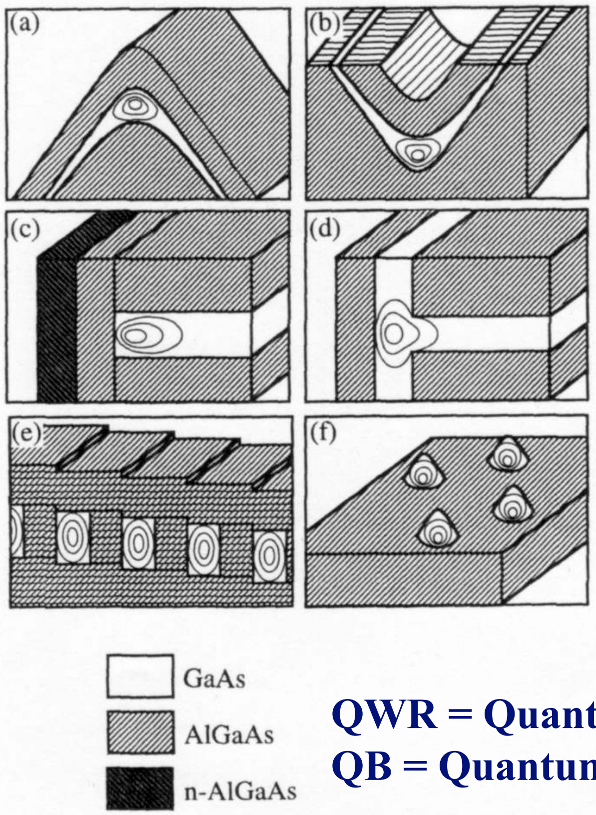

QWR = Quantum Wire
QB = Quantum Box

FIGURE 3. Examples of epitaxially grown QWRs and QBs. A ridge QWR (a), a groove QWR (b), a (field-induced) edge QWR (c), a (T-shaped) edge QWR (d), a tilted superlattice (TSL) (e), and a self-assembled QB structure (f). See section VI.B for their details and references.

G. Timp, *Nanotechnology*, Chapter 5

Patterned substrates:

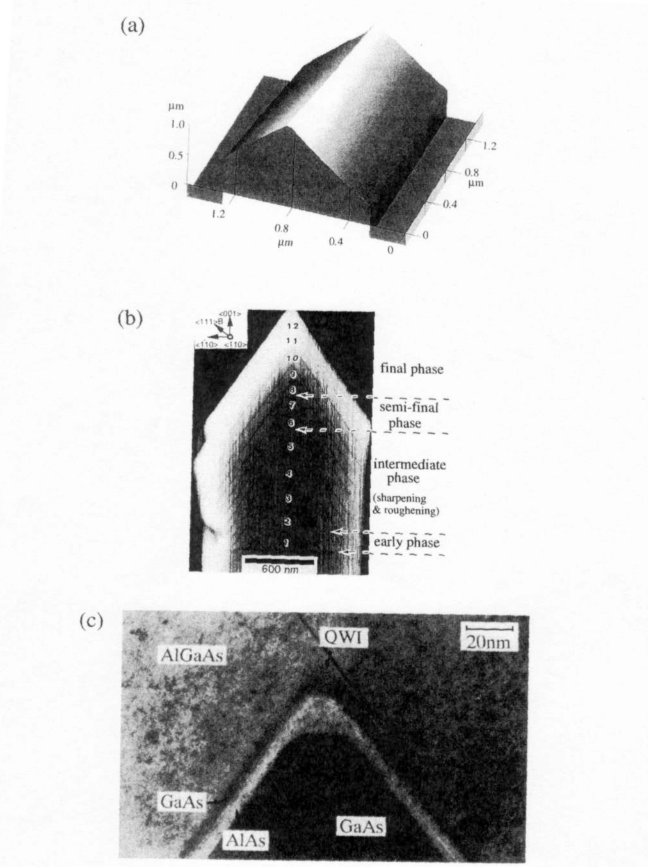

FIGURE 20. (a) An AFM image of an MBE grown *GaAs* ridge. (b)An SEM cross-sectional image of a *GaAs* ridge with thin *AlAs* marker layers. (c)A TEM image of a ridge quantum wire structure after Koshiba *et al.*[97]. (See color plate.)

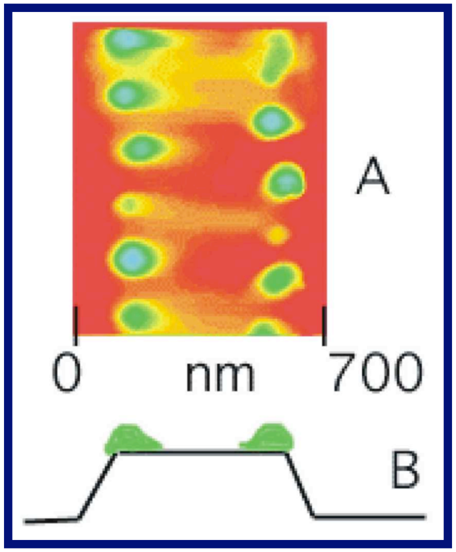

Courtesy of M. Bedzyk

G. Timp, *Nanotechnology*, Chapter 5

Cleaved Edge Overgrowth

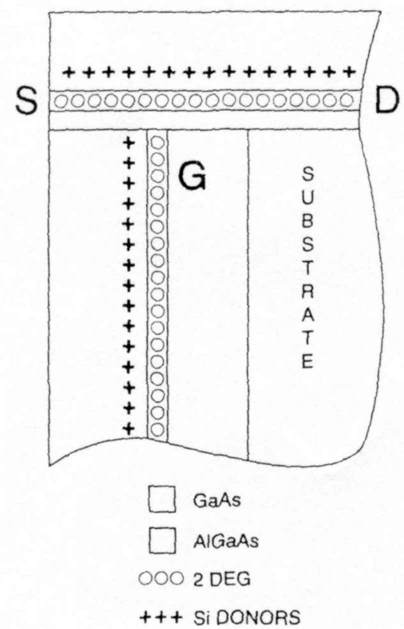

FIGURE 14. The schematic illustration of a novel FET with a 10 nm-long gate, prepared by the cleaved edge overgrowth (after Stormer *et al.*[60]).

G. Timp, *Nanotechnology*, Chapter 5

Self-assembled quantum dots (Ge on Si(001))

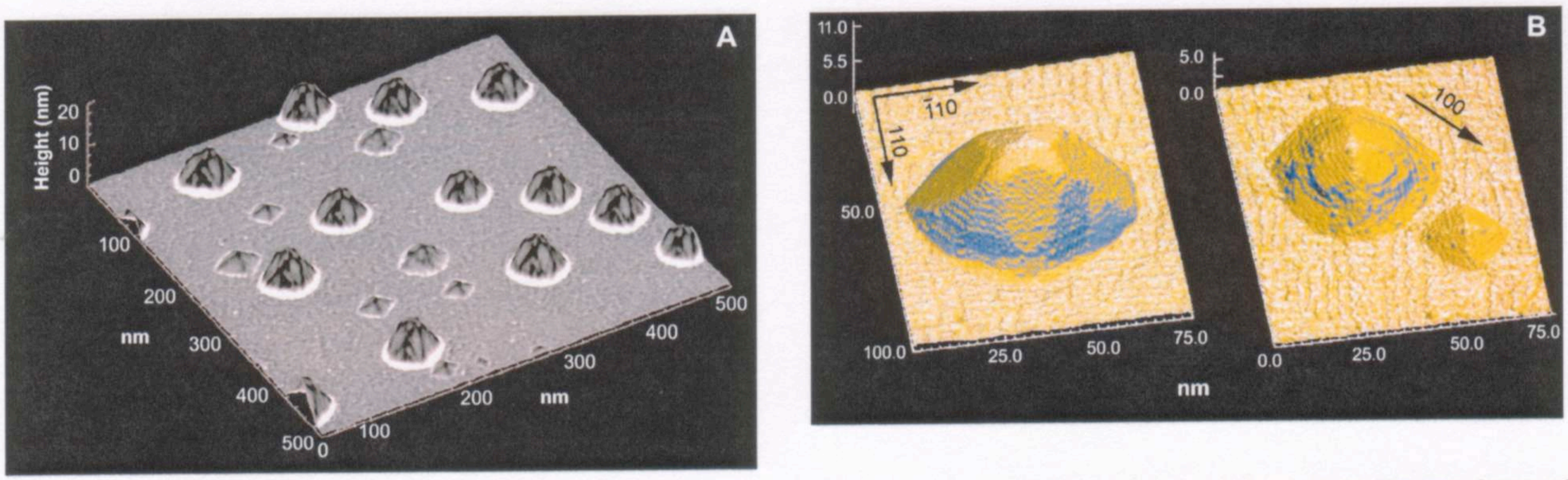

Fig. 1. (**A**) STM topograph [surface height $h(x, y)$ as a function of position] of strained Ge nanocrystals on Si(001), showing both pyramids and domes. The gray scale is proportional to the local surface curvature as determined by the Laplacian $\nabla^2 h(x, y)$: positive curvature is white, flat areas are gray, and negative curvature is black. This visualization mode emphasizes the nanocrystal edges, which appear black and clearly frame the gray facets of the nanocrystals, showing that edges contain a significant fraction of the atoms on the surface of the nanocrystals. (**B**) Higher magnification images of the nanocrystals: (left) a mature dome and (right) a nanocrystal entering the transition stage and a small pyramid.

G. Medeiros-Ribeiro, *et al.*, *Science*, **279**, 353 (1998).

Self-assembled atomic wires (In on Si(001))

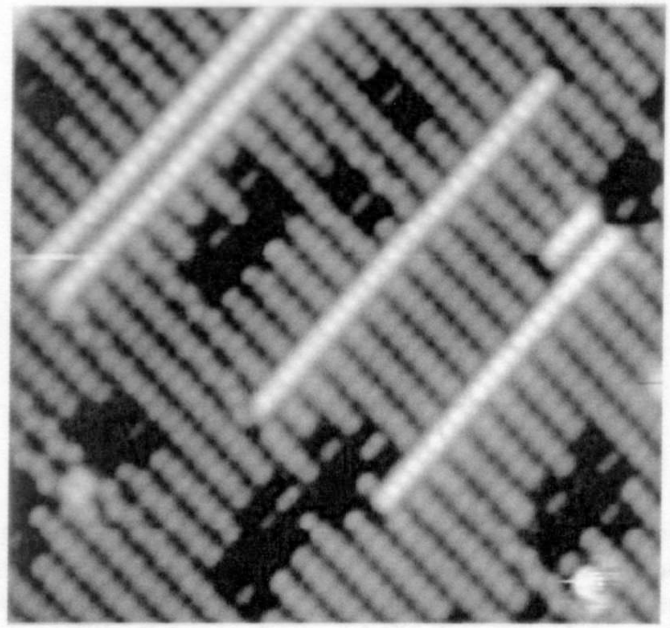

Fig. 2. Filled state STM image of the Si(001) surface with 0.04 ML of In deposited. Several chains of In atoms are visible as bright rows.

J. Nogami, *et al.*, *Surface Review and Letters*, **7**, 555 (2000).

Self-assembled nanowires (silicides on Si(001))

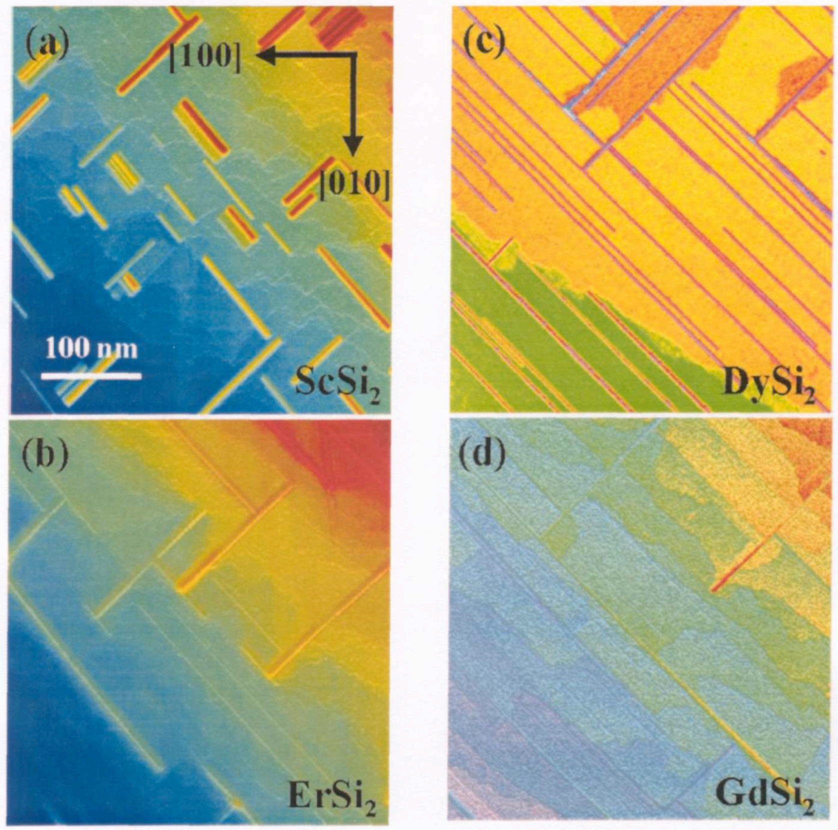

FIG. 3. (Color) STM topographs (400 nm × 400 nm) showing (a) $ScSi_2$, (b) $ErSi_2$, (c) $DySi_2$, and (d) $GdSi_2$ nanowires grown on Si(001) surface shown in Fig. 2. The substrate slopes downward from top right to bottom left with terraces of different heights (in the order of red, green, blue) and are often separated by single atomic steps, but many step bunches can be observed near the ends of the nanowires.

Y. Chen, *et al.*, *J. Appl. Phys.*, **91**, 3213 (2002).

Self-assembled nanowires (silicides on Si(001))

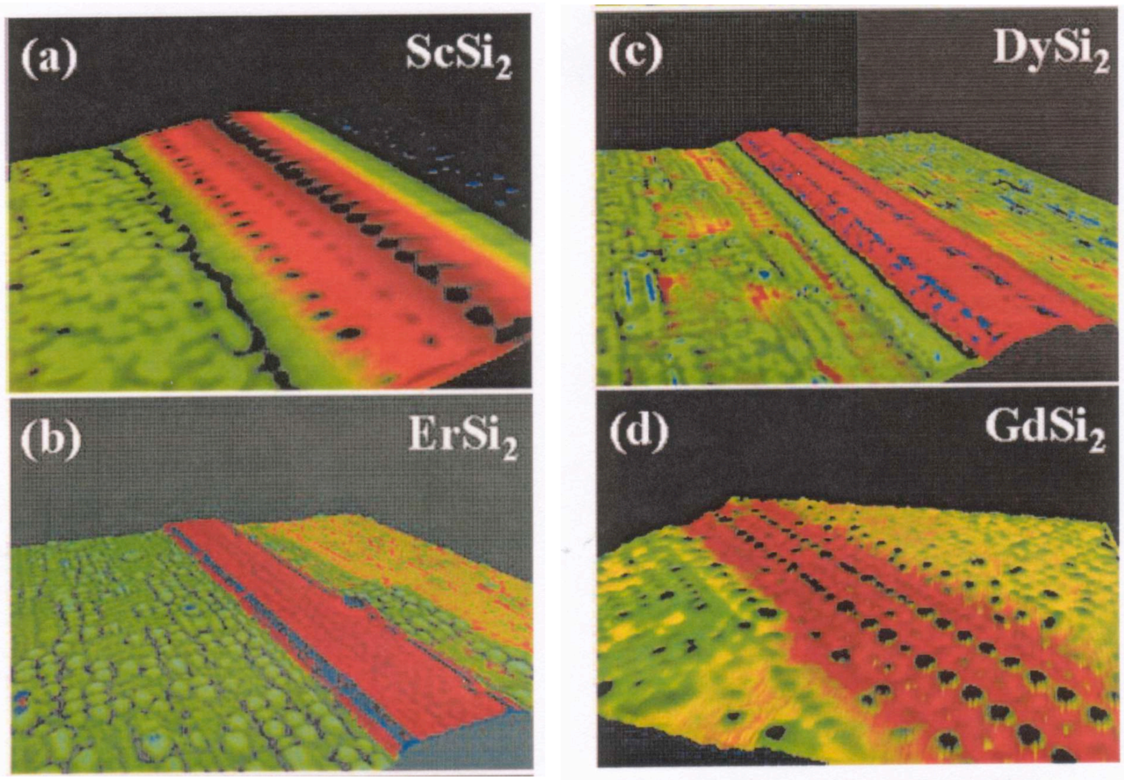

FIG. 5. (Color) High-resolution STM topographs showing sections of (a) a $ScSi_2$ nanowire (width: 13.05 nm, height: 1.79 nm), (b) an $ErSi_2$ nanowire (width: 4.69 nm, height: 0.70 nm), (c) a $DySi_2$ nanowire (width: 4.83 nm, height: 0.56 nm), (d) a $GdSi_2$ nanowire (width: 3.27 nm, height: −0.05 nm, below the Si terrace), as determined by STM, which responds to both geometrical and electronic structure differences.

Y. Chen, *et al.*, *J. Appl. Phys.*, **91**, 3213 (2002).

Self-assembled nanowires (silicides on Si(001))

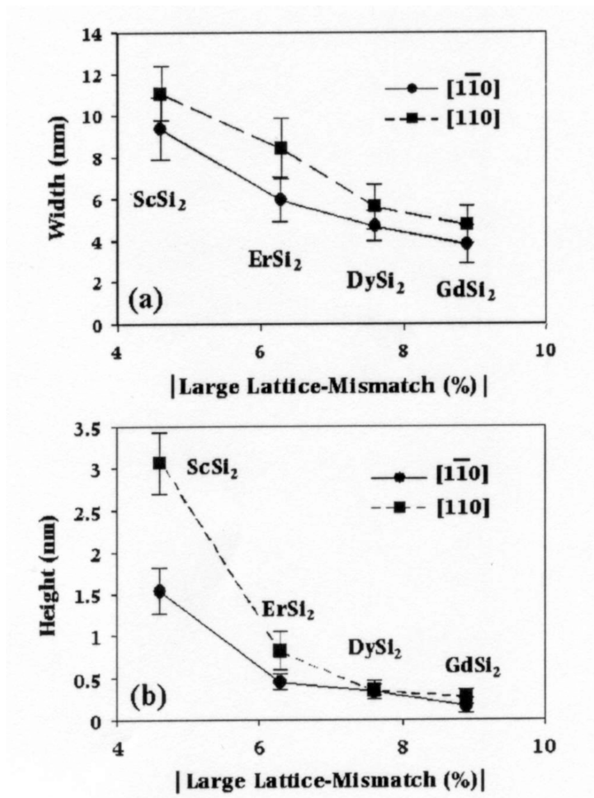

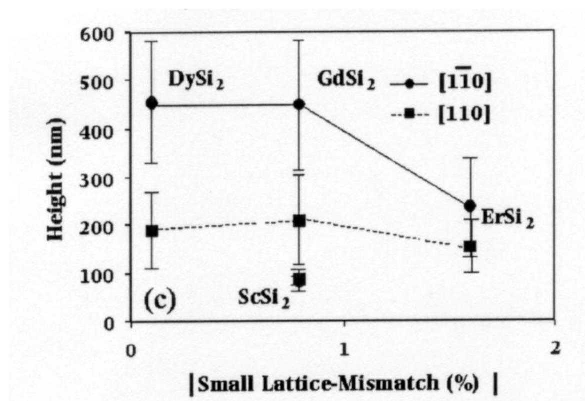

FIG. 4. (a) Average widths vs large lattice mismatches, (b) average heights vs large lattice mismatches, and (c) average lengths vs small lattice mismatches, respectively, of $ScSi_2$, $ErSi_2$, $DySi_2$, and $GdSi_2$ nanowires along $[110]_{Si}$ and $[1\bar{1}0]_{Si}$ directions, respectively. The variation ranges of the nanowire sizes are shown by error bars, which represent standard deviations ($\pm\sigma$) of the data.

Y. Chen, *et al.*, *J. Appl. Phys.*, **91**, 3213 (2002).